University of Denver

Digital Commons @ DU

Electrical and Computer Engineering: Faculty Scholarship | Electrical and Computer Engineering

6-2022

Behavior, Switching Losses, and Efficiency Enhancement Potentials of 1200 V SiC Power Devices for Hard-Switched Power Converters

Ali Mahmoud Salman Al-Bayati
University of Denver

Mohammad Abdul Matin
University of Denver

Follow this and additional works at: https://digitalcommons.du.edu/electrical_engineering_faculty

Part of the Electronic Devices and Semiconductor Manufacturing Commons, and the Power and Energy Commons

Recommended Citation

Al-Bayati, Ali Mahmoud Salman and Matin, Mohammad Abdul, "Behavior, Switching Losses, and Efficiency Enhancement Potentials of 1200 V SiC Power Devices for Hard-Switched Power Converters" (2022). *Electrical and Computer Engineering: Faculty Scholarship*. 52.
https://digitalcommons.du.edu/electrical_engineering_faculty/52

This Article is brought to you for free and open access by the Electrical and Computer Engineering at Digital Commons @ DU. It has been accepted for inclusion in Electrical and Computer Engineering: Faculty Scholarship by an authorized administrator of Digital Commons @ DU. For more information, please contact jennifer.cox@du.edu,dig-commons@du.edu.

Behavior, Switching Losses, and Efficiency Enhancement Potentials of 1200 V SiC Power Devices for Hard-Switched Power Converters

Publication Statement

This article was originally published as:

Al-Bayati, A. M. S., & Matin, M. A. (2022). Behavior, switching losses, and efficiency enhancement potentials of 1200 V SiC power devices for hard-switched power converters. *CPSS Transactions on Power Electronics and Applications*, (7)2, 113-129. doi: 10.24295/CPSSTPEA.2022.00011

Copyright is held by *CPSS Transactions on Power Electronics and Applications (CPSS TPEA)*. This article is shared under CPSS TPEA's Open Access statement:

"All articles which are published in CPSS TPEA are permanently free for everyone to read, download and share."

User is responsible for all copyright compliance.

This article is available at Digital Commons @ DU: https://digitalcommons.du.edu/electrical_engineering_faculty/52

Behavior, Switching Losses, and Efficiency Enhancement Potentials of 1200 V SiC Power Devices for Hard-Switched Power Converters

Ali Mahmoud Salman AL-BAYATI and Mohammad Abdul MATIN

***Abstract*—Semiconductor power devices are the major constituents of any power conversion system. These systems are faced by many circumscriptions due to the operating constraints of silicon (Si) based semiconductors under certain conditions. The emergence and persistence evolution of wide bandgap technology pledge to transcend the restrictions imposed by Si based semiconductors. This paper presents a thorough experimental study and assessment of the performance of three power devices: 1200 V SiC cascode, 1200 V SiC MOSFET, and 1200 V Si IGBT under the same hardware setup. The study aims to capture the major attributes for each power device toward determining their realistic potential applications. The switching performance of each power device is studied and reported. As the gate resistance is a crucial factor in a power device characterization, an extensive analysis of hard-switching losses under different separated turn-on and turn-off gate resistances is also performed and discussed. To appraise the fast switching capability, the switching d*v*/d*ts* and d*i*/d*ts* are measured and analyzed for each power device. Furthermore, insights are provided about the dependency of switching energy losses on the power device current and blocking voltage. This paper also focuses on evaluating the operations and the performances of these power devices in a hard-switched dc-dc converter topology. While using of 1200 V SiC Schottky diode in the converter design with each power device, the high switching frequency operations and efficiency of the converter are reported and thoroughly explored. The SiC cascode exhibited superior performance when compared to the other two power devices. The results and analyses represent guidelines and prospects for designing advanced power conversion systems.**

***Index Terms*—Converter design, device characterization, high efficiency, Si IGBT, SiC cascode, SiC MOSFET, SiC Schottky diode, switching losses, wide bandgap (WBG) technology.**

I. Introduction

WITH the robust economic progress and social welfare in developing countries, the world power consumption trend is in a steadily increasing status [1]. In 2018, the global energy demand was raised up by 2.3% [2]. Thus, power generation using renewable technologies reaped substantial attention not only to supply the increasing energy demand, but also to reduce the world's dependency on traditional use of fossil fuel, mitigating its impact on the environment and climate change. The world total installed capacity of photovoltaic (PV) generation reached 505 GW and 591 GW of wind power by the end of 2018 [3]. In the context of energy conversion systems, where the energy is manipulated and processed, system efficiency is a major concern. This influential importance of the efficiency is not merely related to the matters of thermal design, but as well due to the massive fraction and cost of dissipated energy. Hence, the vital issue is to design such systems with high efficiency power converters and a lower operational power dissipation in order to minimize the total system loss.

Beside the loss and efficiency concerns, high temperature operation as well as high power density are other obstacles that the power converter designers face in multitude applications. As the semiconductor power devices are the major building components of power converters, considerable ameliorations of these devices are indispensable in the matter of power density, high efficiency with less power loss, and cost. The continuous developments for years in silicon (Si) technology led to substantial manufacturing of Si based power devices with low costs, paving the way for these devices to be the dominant option for power converter design. Whereas enhancements stay undergoing [4]–[6], Si based power devices exhibit restricted performance at high values of voltage, temperature, and switching frequency. With the emergence and advances of silicon carbide (SiC) technology in the recent decade, producing of power devices to attain important needs such as higher voltage, higher current, and higher operating temperature became promising. Hence, SiC metal-oxide semiconductor field-effect transistors (MOSFETs) and SiC Schottky diodes initiated to permeate the applications of conventional Si based power devices. The SiC semiconductor physical features compared to Si comprise a larger bandgap energy, higher electric field, and thermal conductivity. Its large bandgap enable SiC power devices to have lower drift region resistance than Si counterparts and to work at higher temperatures, while higher electric field capability leads to smaller size with higher

Manuscript received April 19, 2021; revised July 29, 2021; accepted October 6, 2021. Date of publication June 30, 2022; date of current version June 10, 2022.

A. M. S. Al-bayati is with Department of Electrical and Computer Engineering, University of Denver, 2155 East Wesley Avenue Denver, Denver, Colorado 80210, United States (e-mail: alimahmoudsalman.al-bayati@du.edu).

M. A. Matin is with Daniel Felix Ritchie School of Engineering & Computer Science, University of Denver, 2155 East Wesley Avenue Denver, Denver, Colorado 80210, United States(e-mail: mohammad.matin@du.edu).

Digital Object Identifier 10.24295/CPSSTPEA.2022.00011

doping concentration layer devices. Moreover, power devices made with SiC semiconductor exhibit more efficacious heat dissipation than Si devices as a result of higher thermal conductivity merit of SiC [7], [8]. However, it is worth mentioning that for the same breakdown voltage and current rating, the SiC power device cost is higher compared to Si power device. This is mainly due to the high material cost and low manufacturing revenue [9].

Following the fabrication of the first SiC MOSFET [10], the trend of SiC semiconductors research studies and developments has been significantly increased. All these efforts led not only to the production of several generations of intermediate voltage range single chip controllable SiC power devices [11]–[13], but also manufacturing of SiC power modules has been possible [14], [15].

Device level comparison showed a low reverse recovery current of SiC diode with respect to its counterparts Si diode [16], [17]. This merit drives to a low switching losses of switching devices and can yield major benefits in many applications [18], [19]. Performance improvement of different power converter topologies for various applications using discrete SiC power devices have been researched and discussed [20]–[25]. In most of these works, it has been attempted to deploy these devices to achieve reduced losses to increase the efficiency; high switching frequency for compactness intention; enabling high temperature operation toward a smaller cooling requirements; or even all these targets together. In the context of power modules, developing all SiC based power modules, which are typically packaged from multiple discrete SiC devices, enabled designing of medium voltage as well as high power converter systems [26], [27].

Although the former mentioned studies tried to explore the promises and hype that have been raised about SiC technology, issues such as the future of this technology as well as the propriety of a device for a particular design need to be addressed. The switching characterization of different SiC power devices has been reported in the literature [7], [28]–[30]. However, these characterizations are not thoroughly studied to realize the potential of these devices in the design of power converter systems. A single driving path for device turn-on and turn-off used in these studies where the switching characterization has been reported at only two values of gate resistance in [28] and at different gate resistances in [7], [29], while the author in [30] mentioned to testing different gate resistances in order to identify an optimal driving condition. Unlike these works, a detailed methodology is presented in this paper to quantify the sensitivity and correlation of the gate resistance with the power device behavior during the turn-on and turn-off transitions. This will not only lead to operate a power device under a best driving condition, but it also helps to avoid any switching related issues of a power device. Also, the paper presents comprehensive performance and switching energy losses profiles of the power devices under study captured under separated turn-on and turn-off gate driving paths, which will assist power converter designers to perform better loss expectation and efficiency estimation of hard-switched power converters designed with these power devices. Further, it is important to mention that as new productions of SiC power devices have emerged since these works, it is of interest to study their characteristics and provide their application prospects.

A detailed experimental characterization study as well as an assessment of device performance in a hard-switched power converter system of three power devices are presented in this paper. The main aspirations include quantifying the implications of the gate resistance on the power devices' switching performance, switching energy losses, and switching speeds as well as exploring the potentials of each power device in the operation of a hard-switched power converter. The rest of this paper is organized as follows: Section II introduces the power devices under study along with their specifications. Section III presents the laboratory experiment hardware setup for the power devices' characterization and introduces the followed methodology. Sections IV and V present detailed characterization of the 1200 V, 33 A SiC cascode, 1200 V, 31 A SiC MOSFET, and 1200 V, 30 A Si IGBT using the same hardware setup. Measurements of switching losses at different separated gate resistances for the turn-on and turn-off conditions, switch currents, and voltages are performed and analyzed. Further, detailed switching d*v*/d*ts* and d*i*/d*ts* are measured and reported. In Sections VI and VII, the design of a dc-dc buck converter and its operational performance and efficiency with each power device are presented and studied. Section VIII presents the conclusions of this paper.

II. The Power Devices Under Study

Three power devices are studied under the same hardware setup in this paper. Table I provides the details of each power device. These power devices are selected such that they share the most important criteria from a power converter designer perspective including similarity in blocking voltage level, rated continuous current, maximum junction temperature, and type of packaging. The first power device is a SiC FET from United-SiC Inc. which is based on cascode configuration. The second and third power devices are a SiC MOSFET from ROHM company and a Si IGBT from Infineon Technologies. The SiC MOSFET is among the third generation of ROHM company's SiC MOSFETs and it is based on double-trench structure. Further, a 1200 V SiC Schottky diode is used during the characterization of each power device. This SiC Schottky diode has a merged PIN Schottky structure and it belongs to the fourth generation of Cree company's SiC Schottky diodes. The part number and other specifications of the SiC Schottky diode are also provided in Table I.

III. Laboratory Experiment Hardware Setup for Power Device Characterization and Methodology

Switching performance and loss information of power devices are typically acquired through device characterization process. The significance of such information lies not only in providing a deeper understanding of device behavior, but also helps the designers to optimize the structuring of power

TABLE I
THE PART NUMBER AND SPECIFICATIONS OF THE POWER DEVICES UNDER STUDY

Device technology	SiC cascode	SiC MOSFET	Si IGBT	SiC schottky diode
Manufacturer	UnitedSiC	ROHM	Infineon	CREE
Part number	UJ3C120080K3S	SCT3080KL	IKW15N120H3	C4D15120H
Package type	TO–247	TO–247	TO–247	TO–247
Blocking voltage/ V	1200	1200	1200	1200
Continuous current rating/ A	33	31	30	39
Maximum junction temperature / °C	175	175	175	175

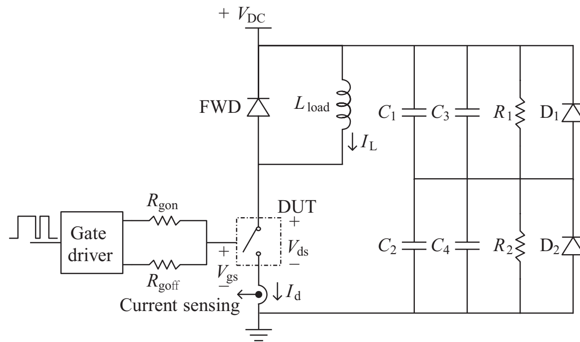

Fig. 1. DPT circuit schematic.

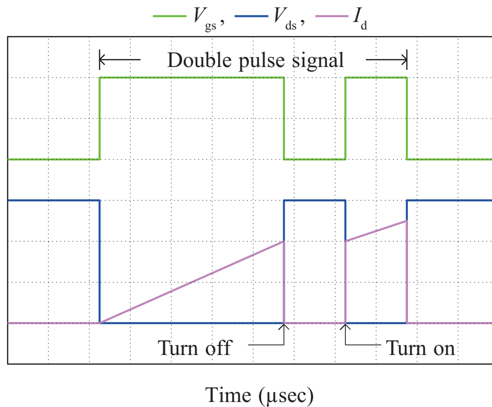

Fig. 2. DPT typical switching waveforms.

converters in terms of making pertinent device choice as well as loss and efficiency estimations. Double pulse test (DPT) is a dominant technique to study the dynamic characteristics of power devices under hard–switching environment [28], [31]. Fig. 1 depicts the circuit schematic of the DPT. The double pulse signal which is supplied to the device under test (DUT) is illustrated in Fig. 2.

A schematic illustration of the DPT experiment setup is depicted in Fig. 3. A dual channel waveform generator from Keysight Technologies, model 33500B, produces controllable widths double pulse signals for the testing system. The gate driver IC 1EDI60I12AH from Infineon is used to drive the power devices. This gate driver is galvanically isolated and can deliver up to 6 A peak current. Moreover, its separated output pins enable to comprehensively study the power devices' behaviors during the turn-on and turn-off transitions at different values of the turn-on, R_{gon}, and turn-off, R_{goff}, gate resistances.

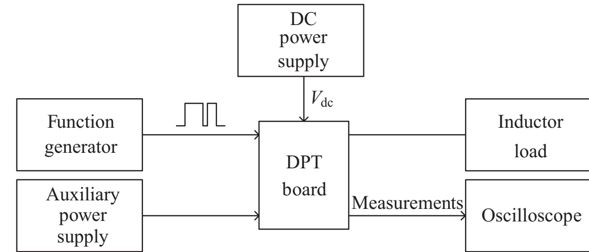

Fig. 3. Schematic illustration of the DPT experiment setup.

Suitable instruments are utilized to capture the DUT's switching waveforms, gate-source voltage (V_{gs}), V_{ds}, and I_d to be observed through an oscilloscope. The load used in the DPT circuit, L_{load}, is an air core inductor of 0.47 mH which is parallel with the top switch as shown in Fig. 1. The capacitor bank, C_1, C_2, C_3, and C_4, is a combination of film and ceramic capacitors with low equivalent series inductance, eletronic system fevel (ESL). It provides the stored energy to the L_{load} as well as it smoothes the applied V_{dc}. The low ESL of the capacitors along with the trace path low inductance ensure a current commutation path with a small parasitic inductance. The resistors, R_1 and R_2, secure balancing the voltage across the energy storage capacitors that are connected in series, while a severe over voltage condition of these capacitors can be protected by the two diodes, D_1 and D_2. The SiC Schottky diode in the Table I is employed as the free wheeling diode (FWD) of the inductive load in the top switch spot and the rest of the switching power devices are installed in the bottom switch position as the DUT switch.

The ultra fast switching transients during the turn-on and turn-off conditions for some power devices impose giving close attention to the probing and measurements setup. The main concerns from the measurements standpoint lie in choosing voltage and current probes with appropriate bandwidth and a proper time aligned of the measured voltage and current waveforms. This meticulous process is of paramount eminence in capturing the detailed behavior of the device as well as to precise measuring of the switching times and energy losses. In this work, measuring instruments with adequate enough bandwidth and accuracy are employed. The voltage measurements for the DUTs are made using a Tektronix P5200A differential probes, while a Pearson current monitor, model 2877, is used to sense the switching currents. Furthermore, the time skew due to the propagation delay variations between the voltage and current probes is other crucial criterion toward precise measurements. The accuracy of power and energy measurements

TABLE II
EQUIPMENT USED IN THE EXPERIMENT

Equipment	Manufacturer	Model	Deskew
Dc power supply	Keysight	N8937A	—
Oscilloscope	Tektronix	DPO3014	with deskew
Voltage probe	Tektronix	P5200A	11 ns
Pearson current sensor	Pearson electronics	2877	0 ns

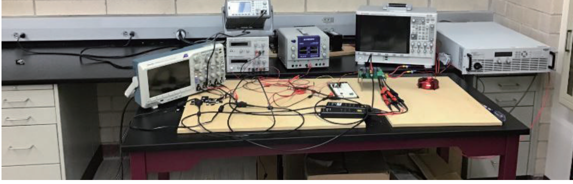

Fig. 4. Laboratory setup of the DPT experiment.

can significantly suffer if there is time misalignment between the probes. Hence, the aforementioned voltage probes are de-skewed in this work with respect to the current sensor to compensate any time delay difference between the measuring instruments. Thus, the results can be obtained precisely. Table II provides the details of the equipment used in the DPT experiment.

Due to the critical role of the gate resistance on a power device switching behavior, an exhaustive characterization study is performed using separated turn-on and turn-off gate driving paths for all the power devices in a systematic manner as it can be seen in Sections IV and V. The main target here is to quantify how sensitive each power device behavior is with the gate resistance during the turn-on and turn-off transients. This will lead to drive a power device in an optimal condition in terms of avoiding any improper device switching and also to operate each power device under a best tradeoff between the switching losses and the voltage and current ringing. Also, this will help to build up switching losses portfolio of each power device that may assist in expectations of switching losses and energy saving.

IV. Experimental Device Switching Characterization

In this section, a hard-switched characterization is performed for the DUT in the configuration illustrated in Fig. 1 using the setup in Fig. 4. The switching performance of all the devices are captured and studied under the same conditions with 800 V dc bus voltage and 20 A of switched current. The test voltage of 800 V is used taking into account the turn-off transition voltage overshoot together with the voltage ripple that arises in several applications. This insures a passable safety margin for the 1.2 kV blocking voltage capability of the device. The main target of this section is to quantify the correlation strength between the dynamic performance of each power device during the turn-on and turn-off transients with the gate resistance. As mentioned earlier, this will not only lead to avert any improper device switching but also it helps to determine adequate tradeoff between the switching losses and the power device voltage and current ringing. In what follows, each DUT is turned on and turned off within its recommended V_{gs} driving

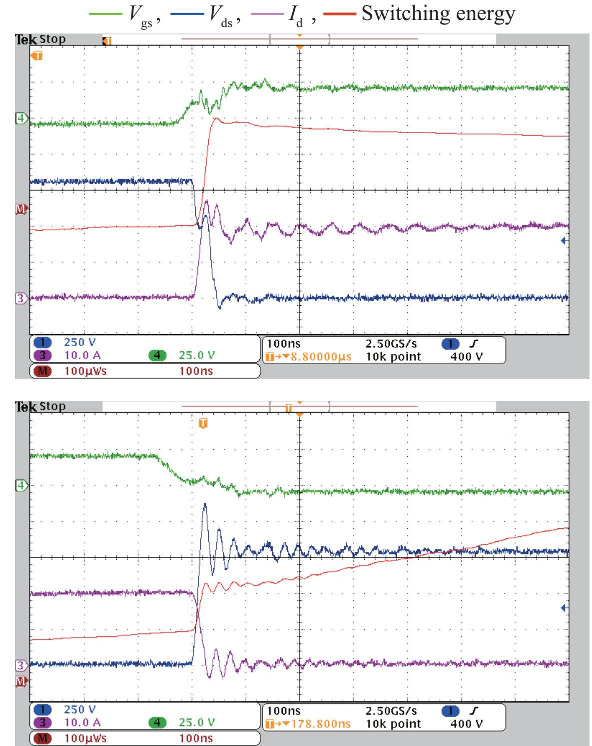

Fig. 5. Switching characteristics of 1200 V SiC cascode at: V_{dc} = 800 V, I_d = 20 A, R_{gon} = 5 Ω, R_{goff} = 15 Ω, V_{gs} = +20/–5 V; Scale: V_{gs} → 25 V/div, V_{ds} → 250 V/div, I_d → 10 A/div, time → 100 ns/div, switching energy → 100 µJ/div. Turn–on transition (top), turn–off transition (bottom).

voltage value. The device turn-on and turn-off switching energy losses are obtained through integrating the multiplication of the measured V_{ds} and I_d waveforms.

A. 1200 V SiC Cascode Switching Characteristics

The 1200 V, 33 A SiC cascode is characterized at room temperature with 800 V of bus voltage and 20 A of switched current using the test circuit in Fig. 1. The device is turned on with +20 V and turned off with –5 V. The gate resistances are selected to be 5 Ω and 15 Ω for the turn-on and turn-off conditions, respectively. The measured switching waveforms are shown in Fig. 5. The switching energy loss during the turn-on transition is measured to be 298 µJ, which is over two times of that during the turn-off transition with 134 µJ. The overshoot in device current during the turn-on transition is due to the junction capacitance of the FWD. On the other hand, a voltage overshoot is observed during the turn-off transition where it is caused by the inductance of the power loop. This power loop inductance is a combination of the parasitic inductance of current commutation path along with the inductance of device package. It is worth to mention that the current commutation path inductance results from the board trace of the current route as well as the current probe, which increases the length of the commutation path. Moreover, a resonance may shape between the power loop inductance and the device stray capacitance that can induce the observed oscillations in the device voltage and current.

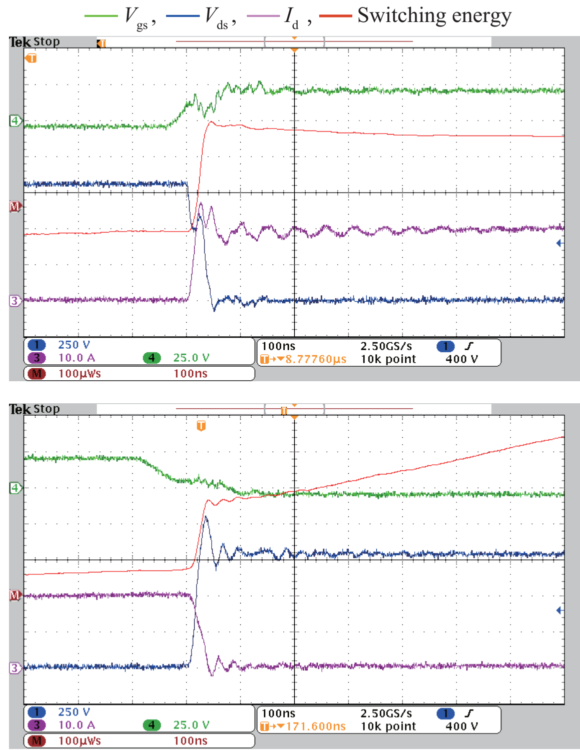

Fig. 6. Switching characteristics of 1200 V SiC cascode at: V_{dc} = 800 V, I_d = 20 A, R_{gon} = 5 Ω, R_{goff} = 30 Ω, V_{gs} = +20/−5 V. Scale: V_{gs} → 25 V/div, V_{ds} → 250 V/div, I_d → 10 A/div, time → 100 ns/div, switching energy → 100 µJ/div. Turn-on transition (top), turn-off transition (bottom).

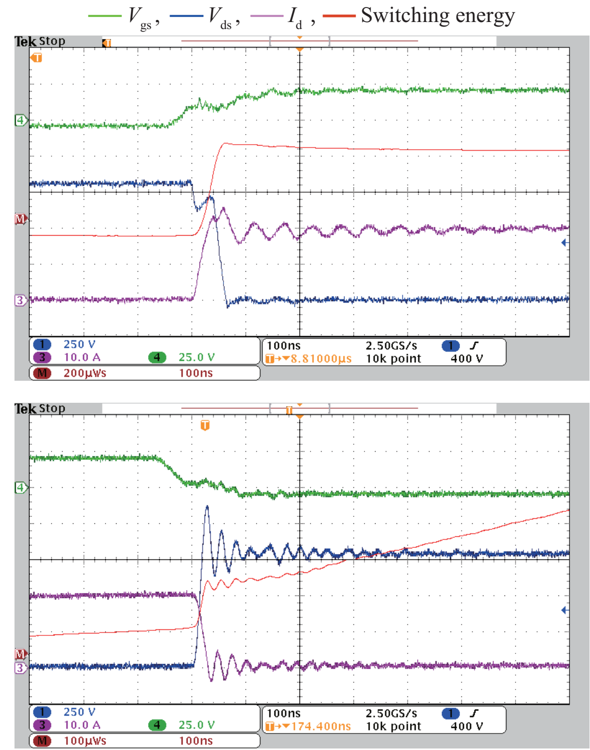

Fig. 7. Switching characteristics of 1200 V SiC cascode at: V_{dc} = 800 V, I_d = 20 A, R_{gon} = 20 Ω, R_{goff} = 15 Ω, V_{gs} = +20/−5 V. Scale: V_{gs} → 25 V/div, V_{ds} → 250 V/div, I_d → 10 A/div, time → 100 ns/div, turn–on switching energy → 200 µJ/div, turn-off switching energy → 100 µJ/div. Turn-on transition (top), turn-off transition (bottom).

As mentioned earlier, there is a strong relationship between the gate resistance, the device voltage and current ringing, and the switching energy losses. Hence, the impacts of separated R_{gon} and R_{goff} on the switching performance are reported in this paper, which are not comprehensively presented in previous works. This can provide important insights toward optimal design of the converters in terms of minimizing switching energy losses with acceptable ringing of the device voltage and current. A test procedure is carried out by increasing only the R_{goff} and keeping the R_{gon} the same, and vice versa. The switching characteristics are compared in terms of energy losses, voltage and current ringing, and their overshoot. Fig. 6 shows the measured switching performance when the R_{goff} is doubled to 30 Ω while the R_{gon} is kept at 5 Ω. Also, the same other test condition in Fig. 5 is maintained. The turn-on and turn-off transitions switching energy losses are 306 µJ and 194 µJ, respectively. With comparison to the previous case, a very slight increasing is observed in the turn-on energy loss, however, the turn-off energy loss is increased significantly over 44.77%. The turn-on characteristics are almost the same compared to the previous case, however, voltage overshoot and ringing are reduced during the turn-off transition. It can be considered that the reduction in turn-off voltage overshoot and ringing is a minor factor with comparison to the considerable increase of the turn-off energy loss.

Fig. 7 shows the captured switching characteristics with 20 Ω of R_{gon} and 15 Ω of R_{goff}. In comparison with the first case, the turn-on transition switching energy loss is 512 µJ and 132 µJ is the turn-off transition switching energy loss. Over 71.81% is the amount of increase in the turn-on transition switching energy loss with negligible change in the turn-off transition loss. In the context of overshoot, the turn-off waveforms are nearly the same while small overshoot reduction is noted in the turn-on current. This small reduction in the current overshoot is less significant when compared to the substantial increasing of total switching energy loss. Hence, it is crucial for the power converter designer to mitigate the device voltage and current ringing through lowering the current commutation route stray inductance.

B. 1200 V SiC MOSFET Switching Characteristics

Using the same test circuit in Fig. 1, characterization is carried out of the 1200 V, 31 A SiC MOSFET at room temperature with bus voltage of 800 V and 20 A of switched current. The gate voltage of +15 and –3 V is used to turn on and off the device, respectively. A 5 Ω gate resistance is used for the turn-on transition while the gate resistance for the turn-off transition is 15 Ω. Fig. 8 shows the turn-on and turn-off switching waveforms of the device. The measured turn-on transition switching energy loss is 1.36 mJ and the turn-off transition switching energy loss is 426 µJ. It can be noted that the turn-on transition energy loss is more than 3 times higher than the energy loss during the turn-off transition. Due to the inductance of current commutation path, a drop as well as an overshoot in the device

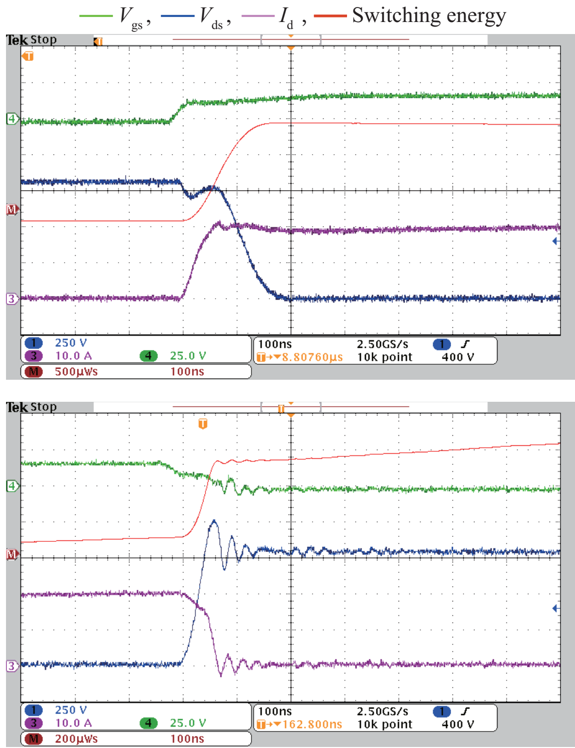

Fig. 8. Switching characteristics of 1200 V SiC MOSFET at: V_{dc} = 800 V, I_d = 20 A, R_{gon} = 5 Ω, R_{goff} = 15 Ω, V_{gs} = +15/−3 V. Scale: V_{gs} → 25 V/div, V_{ds} → 250 V/div, I_d → 10 A/div, time → 100 ns/div, turn-on switching energy → 500 µJ/div, turn-off switching energy → 200 µJ/div. Turn-on transition (top), turn-off transition (bottom).

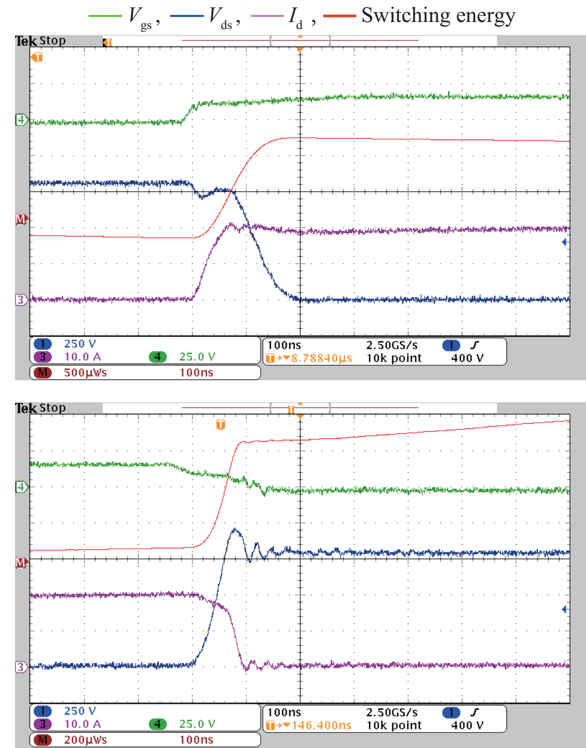

Fig. 9. Switching characteristics of 1200 V SiC MOSFET at: V_{dc} = 800 V, I_d = 20 A, R_{gon} = 5 Ω, R_{goff} = 30 Ω, V_{gs} = +15/−3 V. Scale: V_{gs} → 25 V/div, V_{ds} → 250 V/div, I_d → 10 A/div, time → 100 ns/div, turn-on switching energy → 500 µJ/div, turn-off switching energy → 200 µJ/div. Turn-on transition (top), turn-off transition (bottom).

voltage are observed during the turn-on and turn-off transitions, respectively.

The same test procedure is followed to explore the effect of gate resistances on the switching performance of the device. The switching waveforms are measured with 30 Ω of R_{goff} and 5 Ω of R_{gon} with other conditions remaining the same as shown in Fig. 9. It is found that the turn-off transition energy loss is increased by 38.96% to be 592 µJ than that obtained in Fig. 8. However, the turn-on transition energy loss is found to be 1.39 mJ, exhibiting a very small increase over the previous case. In contrast, there is no major variation in the turn-on waveforms, while the voltage overshoot and current ringing are lowered during the turn-off transition.

Also, the switching characteristics are measured when the R_{gon} is increased to 20 Ω and the R_{goff} is maintained at 15 Ω. The obtained switching waveforms are shown in Fig. 10. The measured turn-on and turn-off transitions energy losses are 1.97 mJ and 420 µJ, respectively. Comparing with the results in Fig. 8, a negligible change is observed in the turn-off transition energy loss, while an increase of more than 44.85% is occurred in the turn-on transition energy loss. On the other hand, it can be seen that the switching waveforms are roughly the same despite the aforementioned change in the R_{gon}.

C. 1200 V Si IGBT Switching Characteristics

Under 800 V of dc bus voltage and 20 A of switched current, the 1200 V, 30 A Si IGBT is characterized at room temperature

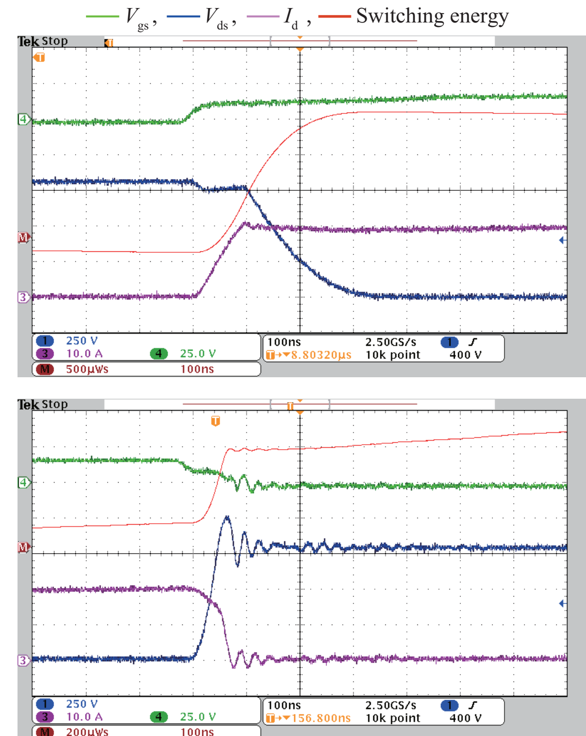

Fig. 10. Switching characteristics of 1200 V SiC MOSFET at: V_{dc} = 800 V, I_d = 20 A, R_{gon} = 20 Ω, R_{goff} = 15 Ω, V_{gs} = +15/−3 V. Scale: V_{gs} → 25 V/div, V_{ds} → 250 V/div, I_d → 10 A/div, time → 100 ns/div, turn-on switching energy → 500 µJ/div, turn-off switching energy → 200 µJ/div. Turn-on transition (top), turn-off transition (bottom).

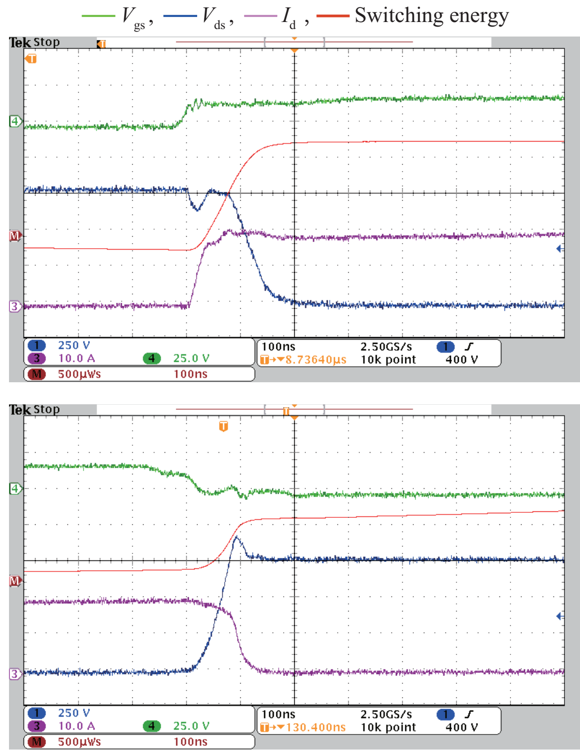

Fig. 11. Switching characteristics of 1200 V Si IGBT at: V_{dc} = 800 V, I_d = 20 A, R_{gon} = 5 Ω, R_{goff} = 15 Ω, V_{gs} = +15/−5 V. Scale: V_{gs} → 25 V/div, V_{ds} → 250 V/div, I_d → 10 A/div, time → 100 ns/div, turn-on switching energy → 500 µJ/div, turn-off switching energy → 500 µJ/div. Turn-on transition (top), turn-off transition (bottom).

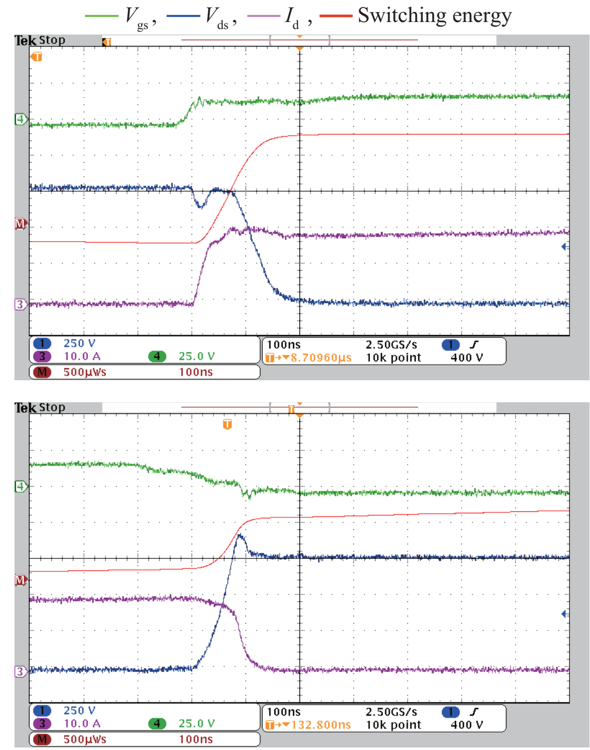

Fig. 12. Switching characteristics of 1200 V Si IGBT at: V_{dc} = 800 V, I_d = 20 A, R_{gon} = 5 Ω, R_{goff} = 30 Ω, V_{gs} = +15/−5 V. Scale: V_{gs} → 25 V/div, V_{ds} → 250 V/div, I_d → 10 A/div, time → 100 ns/div, turn-on switching energy → 500 µJ/div, turn-off switching energy → 500 µJ/div. Turn-on transition (top), turn-off transition (bottom).

using the same test circuit in Fig. 1. The gate driving condition is used as +15 V for turning-on and –5 V for turning-off the device along with 5 Ω of R_{gon} and 15 Ω of R_{goff}. The switching waveforms are captured and shown in Fig. 11. The measured switching energy loss during the turn-on transition is 1.48 mJ, whereas the energy loss during the turn-off transition is found to be 708 µJ. It can be seen that there is a voltage dip during the turn-on transition as well as a voltage overshoot during the turn-off transition. As in the previous devices, this is due to the parasitic inductance of the current commutation channel.

To better understand the relation between the R_{goff} and the Si IGBT characteristics, the device is examined at 30 Ω of R_{goff} and 5 Ω of R_{gon} while all other conditions are kept the same. Fig. 12 shows the measured switching waveforms. With comparison to the results obtained in Fig. 11, the energy losses during the turn-on and turn-off transitions are measured to be 1.49 mJ and 716 µJ, respectively. It can be noted that a minor increase in the turn-off transition energy loss occurs even with the considerable increasing of the R_{goff}. This means that the turn-off transition of the Si IGBT is not constrained by the variation in gate resistance. Furthermore, no significant improvement occurs in the turn-off voltage overshoot, whereas the turn-on transition voltage dip is because of the parasitic inductance of the current commutation channel.

By increasing the R_{gon} to 20 Ω and maintaining the rest of the test conditions in Fig. 11, the switching characteristics is measured and shown in Fig. 13. The measured turn-on and turn-off

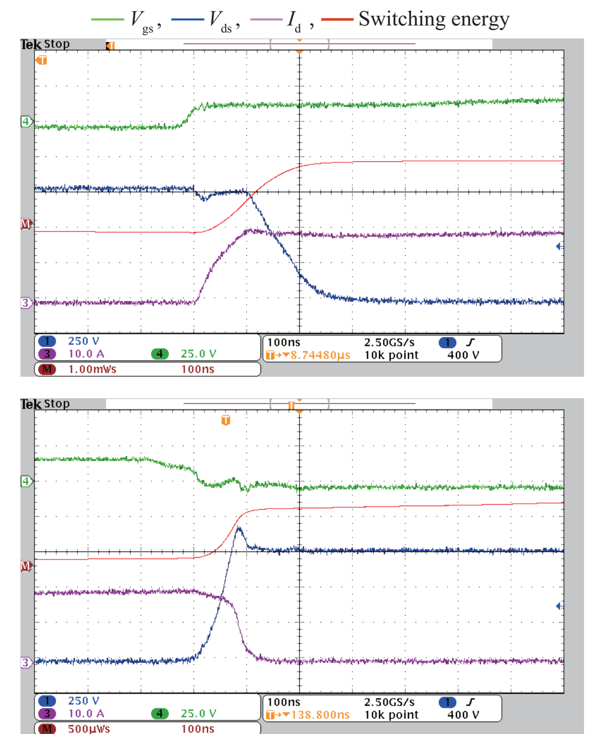

Fig. 13. Switching characteristics of 1200 V Si IGBT at: V_{dc} = 800 V, I_d = 20 A, R_{gon} = 20 Ω, R_{goff} = 15 Ω, V_{gs} = +15/−5 V. Scale: V_{gs} → 25 V/div, V_{ds} → 250 V/div, I_d → 10 A/div, time → 100 ns/div, turn-on switching energy → 500 µJ/div, turn-off switching energy → 500 µJ/div. Turn-on transition (top), turn-off transition (bottom).

transitions are found to be 1.98 mJ and 704 μJ, respectively. There is an over 33.78% increase in the turn-on transition energy loss is observed compared to the results obtained in Fig. 11. Furthermore, it can be seen that the turn-on voltage dip is reduced with the increasing of R_{gon}, however, no momentous changes are observed in the turn-off waveforms.

D. Comparison of Switching Waveforms

In addition to the considered gate resistance values in the previous subsections, the dynamic performance of the power devices under study are also tested under various other values of the R_{gon} and R_{goff}. The importance of this procedure is that it enables to perform a roughly comparison between the power devices considering the internal gate resistance values. Further, conducting the measurements under the same test setup and identical operational condition is the other key factor that helps to carry out such comparison. The results presented in the previous subsections demonstrated that there are negligible impacts of the variations of R_{gon} and R_{goff} on the turn-off and turn-on switching waveforms of the power devices, respectively. In other words, the turn-on characteristics of each power device have a negligible correlation with the R_{goff}, and vice versa. Therefore, for example, to account for the 4.5 Ω and 12 Ω of internal gate resistance values of the SiC cascode and SiC MOSFET, respectively, the turn-on characteristics of the SiC cascode at R_{gon} of 15 Ω can be nearly compared to that of the SiC MOSFET at R_{gon} of 5 Ω. Under this consideration, it is found that the current of the SiC cascode (with aggregate turn-on gate resistance of 19.5 Ω) is rising with a speed about 0.842 kA/μs during the turn-on transition, however, the turn-on current speed is measured to be 0.432 kA/μs for the SiC MOSFET (with aggregate turn-on gate resistance of 17 Ω). In the same manner, the turn-off characteristics can be nearly compared at R_{goff} values of 15 Ω and 5 Ω of the SiC cascode and SiC MOSFET, respectively. The measurements are revealed that the SiC cascode switches with 53.333 kV/μs (with aggregate turn-off gate resistance of 19.5 Ω) while the SiC MOSFET switches with 24.615 kV/μs (with aggregate turn-off gate resistance of 17 Ω). This clearly shows the faster turn-on and turn-off switching capabilities of the SiC cascode compared to the SiC MOSFET even at relatively higher aggregated turn-on or turn-off gate resistance. It is worth mentioning that the SiC cascode exhibits a larger voltage overshoot during the turn-off transition. This is due to the higher turn-off current speed of this device compared to the other two power devices.

V. Switching Losses and Speeds Analysis and Comparison

A comprehensive analysis of switching energy losses and switching speeds for all the power devices under study is presented in this section. In order to adequately quantify the impacts of the gate resistance on the switching energy losses and dynamic behavior of each power device, variations in the R_{gon} and R_{goff} are carried out in a separated manner. Firstly, the R_{goff} is maintained constant at 5 Ω and the R_{gon} is varied within a range of 5 Ω to 25 Ω. Then in a similar procedure, the R_{goff} is increased with the same range while the R_{gon} is kept unchanged at 5 Ω. The followed procedure also allows to perform a roughly fair comparison between the power devices taking into account the internal gate resistances. Furthermore, the analysis includes the study of the loss profile of each power device under different switching voltages and currents.

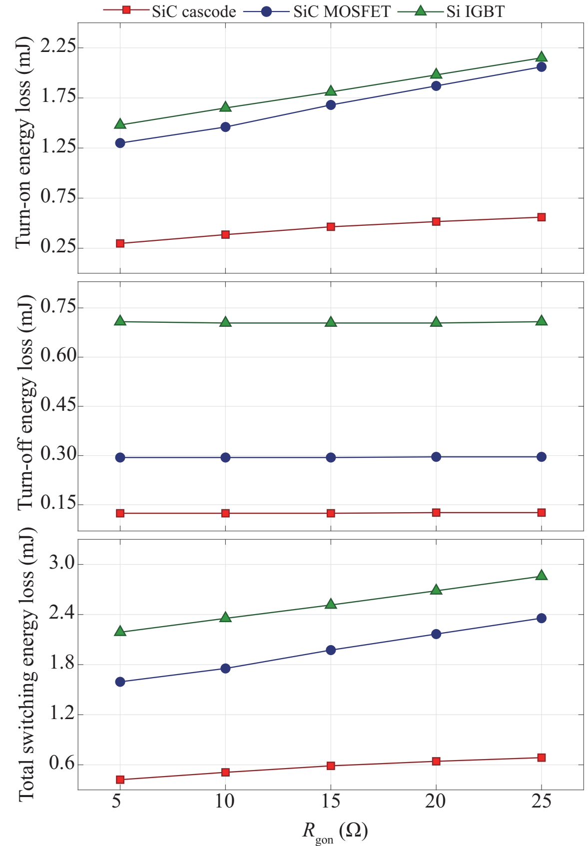

Fig. 14. Switching energy losses versus turn-on gate resistance at: V_{dc} = 800 V, I_d = 20 A, V_{gs} = +20/−5 V for the SiC cascode, V_{gs} = +15/−3 V for the SiC MOSFET, V_{gs} = +15/−5 V for the Si IGBT. Turn-on energy loss (top), turn-off energy loss (middle), total switching energy loss (bottom).

Fig. 14 shows the turn-on, turn-off, and total switching energy losses for all of the devices at different R_{gon} values and fixed 5 Ω of R_{goff}. The measurements are performed at room temperature under a test condition of 800 V dc bus voltage, 20 A of switched current, and with the same aforementioned gate voltage for each device. It is shown that, the turn-on energy loss increases significantly with the elevation of the R_{gon} for all the devices. As the R_{gon} increases from 5 Ω to 25 Ω, the percentage increase of the turn-on energy loss is found to be over 45.27%, 58.46% , and 87.91% for the Si IGBT, SiC MOSFET, and SiC cascode, respectively. This reveals that further lowering of the R_{gon} of the Si IGBT and SiC MOSFET will lead to an insignificant decrease of the turn-on energy loss in comparison to the considerations of voltage and current ringing. Hence, under the same thermal design condition, the SiC cascode can operate at a much higher switching frequency compared to the Si IGBT and SiC MOSFET. Also, negligible very slight changes are observed in the turn-off energy loss of the power devices due to the fixed value of R_{goff}.

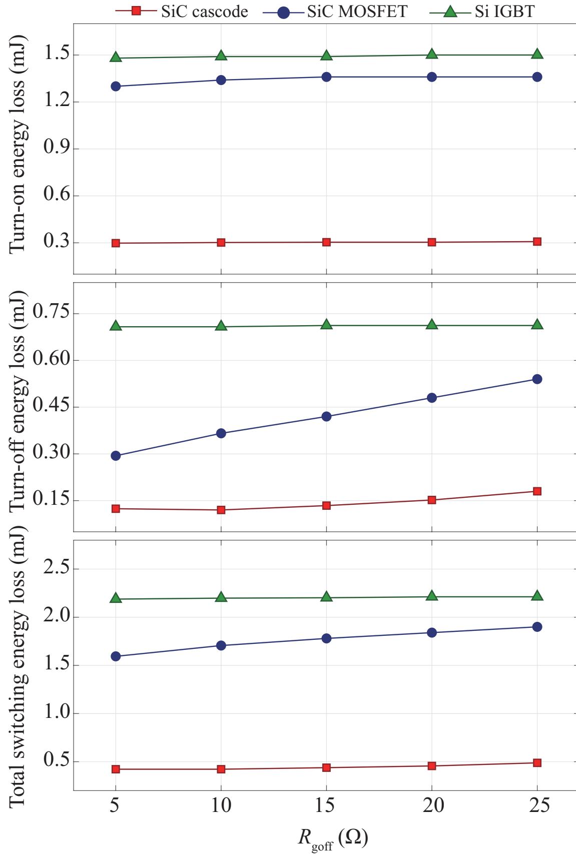

Fig. 15. Switching energy losses versus turn-off gate resistance at: V_{dc} = 800 V, I_d = 20 A, V_{gs} = +20/−5 V for the SiC cascode, V_{gs} = +15/−3 V for the SiC MOSFET, V_{gs} = +15/−5 V for the Si IGBT. Turn-on energy loss (top), turn-off energy loss (middle), total switching energy loss (bottom).

With a 5 Ω fixed R_{gon}, the turn-on, turn-off, and total switching energy losses for all of the devices are captured at different values of R_{goff} as shown in Fig. 15. Each power device is turned on and off at room temperature using its own gate voltage as described previously under a dc bus voltage of 800 V and switched current of 20 A. Specifically, the SiC MOSFET experiences a considerable decreasing in the turn-off energy loss as the R_{goff} decreases. Conversely, it can be seen that the turn-off energy loss of the Si IGBT is nearly constant with the R_{goff} variations. This indicates that the major portion of the turn-off energy loss of the Si IGBT is mainly generated by the tail current with a minor effect of the R_{goff}. The high charge carrier lifetime of the IGBT leads to a relatively considerable current tailing period during the turn-off transition which depends in turn on removing the remaining charge carriers from the *n*–base region through the recombination mechanism in the device [32]. The SiC cascode, on the other hand, shows a rate of decreasing in the turn-off energy loss less than that of the SiC MOSFET. As in the previous case, negligible very limited changes are noted in the turn-on energy loss for all of the power devices as there was no change in the R_{gon} value. It should be noted that from Figs. 14 and 15 that the turn-on energy loss for each power device under study is higher than the turn-off energy loss, which can be taken into account as a vital aspect in power converters' thermal design and management.

TABLE III
Total Switching Energy Loss Reduction With the Variation of R_{gon} and R_{goff} of the Power Devices

Description	SiC cascode	SiC MOSFET	Si IGBT
Reduction in the total switching energy loss as R_{gon} decreases from 25 to 5 Ω and 5 Ω of R_{goff}	38.483%	32.342%	23.442%
Reduction in the total switching energy loss as R_{goff} decreases from 25 to 5 Ω and 5 Ω of R_{gon}	13.524%	16.105%	1.084%

As can be seen from Figs. 14 and 15, there is a strong relation among the gate resistance and the energy losses during the turn-on and turn-off transitions of the SiC cascode and SiC MOSFET. Such a vigorous trend also exists in the turn-on energy loss of the Si IGBT, but with relatively less attitude in the turn-off energy loss. Table III provides the rate of reduction in the total switching energy loss with the variations of the R_{gon} and R_{goff}. It can be seen that the total switching energy loss is positively correlated to the R_{gon} rather than the R_{goff}. This is mainly due to the largest portion of the total switching energy loss is contributed by the turn-on energy loss. Further, as in the previous section, the internal gate resistances can be taken into account to perform a roughly fair comparison between the power devices in terms of the energy losses during the turn-on and turn-off transients. As an example, given that the internal gate resistance values are 4.5 Ω and 12 Ω of the SiC cascode and SiC MOSFET, respectively, the turn-on energy loss of the SiC cascode in Fig. 14 at 15, 20, and 25 Ω of R_{gon} can be nearly compared to that of the SiC MOSFET at R_{gon} values of 5, 10 , and 15 Ω, respectively. In a similar manner, the turn-off energy loss of the SiC cascode in Fig. 15 at 15, 20, and 25 Ω of R_{goff} can nearly be compared to that of the SiC MOSFET at R_{goff} values of 5, 10, and 15 Ω, respectively. Generally speaking, the SiC cascode exibits a superiority againt the other two power devices in terms of lowest energy loss during the turn-on and turn-off transitions, and thereby shows the lowest total switching energy loss.

The variation of the turn-on and turn-off d*v*/d*t* and d*i*/d*t* of all of the power devices with the changes of the R_{gon} and fixed 5 Ω of R_{goff} are measured as shown in Figs. 16 and 17, respectively. It can be seen that, both the d*v*/d*t* and d*i*/d*t* during the turn-on transition of all the power devices, are increasing significantly as the R_{gon} decreases. On the other hand, slight changes are observed in the switching speeds during the turn-off transition due to the fixed value of R_{goff}. Generally speaking, the lower the R_{gon}, the faster the turn-on switching speed and the lower turn-on energy loss. However, a close attention should be given by the power converter designer to other critical issues that could arise from lowering the gate resistance. Such issues include device voltage and current ringing that occur in most power devices, as well as increased electromagnetic interface specifically in the SiC MOSFET [33].

Fig. 18 shows the turn-off d*v*/d*t* and d*i*/d*t* versus the R_{goff} variation for each power device at a constant 5 Ω of R_{gon}. The turn-off d*v*/d*t* and d*i*/d*t* increases with the decrease of the R_{goff} as expected. However, the rate of increasing in this case is

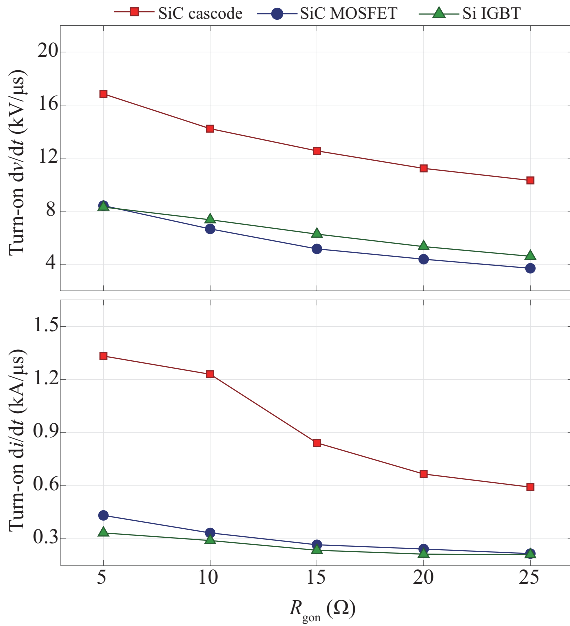

Fig. 16. Turn-on dv/dt and di/dt versus the turn-on gate resistance at: V_{dc} = 800 V, I_d = 20 A, V_{gs} = +20/−5 V for the SiC cascode, V_{gs} = +15/−3 V for the SiC MOSFET, V_{gs} = +15/−5 V for the Si IGBT. Turn-on dv/dt (top), turn-on di/dt (bottom).

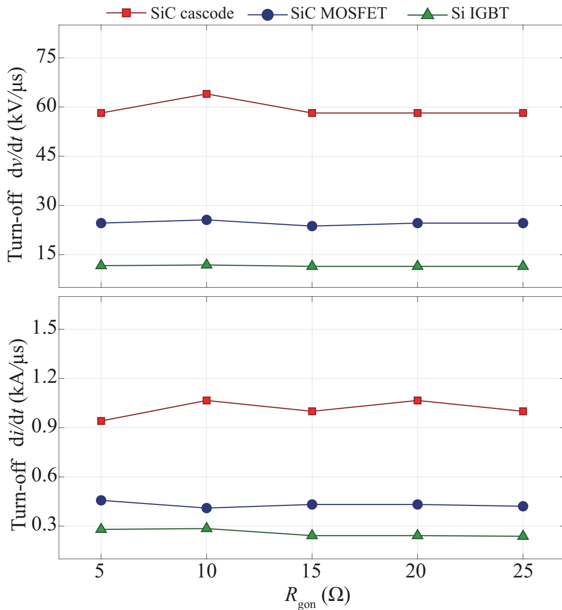

Fig. 17. Turn-off dv/dt and di/dt versus the turn-on gate resistance at: V_{dc} = 800 V, I_d = 20 A, V_{gs} = +20/−5 V for the SiC cascode, V_{gs} = +15/−3 V for the SiC MOSFET, V_{gs} = +15/−5 V for the Si IGBT. Turn-off dv/dt (top), turn-off di/dt (bottom).

remarkably less in comparison to the turn-on dv/dt and di/dt increases that is achieved with the R_{gon} decreasing as in Fig. 16. This manifests that the correlation between the turn-off switching speed and the R_{goff} is comparatively less than that between the turn-on switching speed and the R_{gon}. Moreover, it can be seen that the gate resistance has a limited impact on the switching speed of the Si IGBT during the turn-off transition. Also, the turn-on switching speeds are changed insignificantly as the R_{gon} is kept constant at 5 Ω.

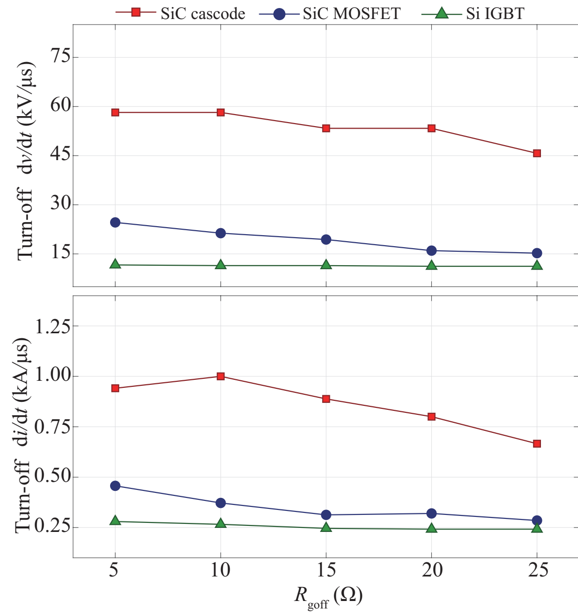

Fig. 18. Turn-off dv/dt and di/dt versus the turn-off gate resistance at: V_{dc} = 800 V, I_d = 20 A, V_{gs} = +20/−5 V for the SiC cascode, V_{gs} = +15/−3 V for the SiC MOSFET, V_{gs} = +15/−5 V for the Si IGBT. Turn-off dv/dt (top), turn-off di/dt (bottom).

The switching speeds can also nearly be compared between the power devices taking into account the internal gate resistances in the same previously mentioned way of switching energy losses' comparison. In overall, it can be clearly seen from Figs. 16, 17, and 18 that the SiC cascode has the fastest switching capabilities during both the turn-on and turn-off transitions. This fastest switching capabilities of the SiC cascode can result in a substantial decrease in the reactive components' size, weight, and cost. Thereby it helps to increase the power density to size ratio of the power converters. However, the high values of dv/dts and di/dts associated with the fast switching may cause serious voltage and current oscillations that could negatively affect the power device reliability. At high dv/dts and di/dts values, the parasitic inductance of the power loop, which includes the inductance of board copper traces as well as the inductance of power device package, may resonates with the power device parasitic capacitance and results in undesirable voltage and current oscillations during the turn-on and turn-off transitions. Such issue will limit the switching speed capabilities of the SiC cascode and thereby increase its switching energy losses. Even though the device voltage and current oscillations can be mitigated through increasing the gate resistance value, this approach may not be highly preferred as it will be at the cost of switching energy losses. Thus, to fully benefit from the fast switching capabilities of the SiC cascode without increasing the switching energy losses, it is important to minimize both the inductance of board copper traces as well as the inductance of the device package.

The SiC cascode and SiC MOSFET offer controllability of the dynamic behavior during the turn-on and turn-off transitions through the gate resistance. However, the Si IGBT exhibits only controllability of the turn-on dynamic behavior through the gate resistance. Hence, the gate resistance plays a

critical role in operating a power device under a best possible driving condition. It is worth mentioning that the SiC cascode in Fig. 15 exhibits a lowest turn-off energy loss at 10 Ω of R_{goff}. Such event is also confirmed in Fig. 18, where the SiC cascode also shows highest turn-off switching speeds at R_{goff} of 10 Ω. This represents an interesting point for further research where it implies that there could be a gate resistance at which the SiC cascode under study may exhibit highest switching speeds with lowest switching energy losses. Here, the 10 Ω of R_{goff} may represent a proper value at which the gate capacitance of the SiC cascode discharge during the turn-off transition. It is important mentioning that selection of a gate resistance should be based on a systematic procedure that ensures less switching energy losses and fast switching with safe and reliable operation.

It is important to note from Figs. 16 and 17 that, at some particular values of R_{gon}, the di/dt during the turn-off transition is greater than that during the turn-on transition. The high turn-off di/dt drives to many major issues of the switching process of a power device. For instance, it may force the turn-off current to ringing status especially for power devices with large value of drain to source capacitance. Consequently, the power device may switch improperly due to the gate voltage oscillations that arise from the stray inductance voltage ringing of the source that results in turn from a high turn-off di/dt. Thus, lowering the turn-off di/dt value is a critical factor toward overcoming the previously mentioned issues. This can be achieved by making the R_{goff} larger than the R_{gon}. This will not impact the power devices' energy loss significantly due to the main portion of the total switching energy loss of the power devices under study comes from the turn-on energy loss rather than the turn-off energy loss. Therefore, the value of the R_{goff} of all the power devices is selected to be 15 Ω. Also, based on the presented analyses and considerations of the switching energy losses and switching speeds, the R_{gon} value of the power devices is selected to be 5 Ω. Here, it is worth mentioning that the R_{gon} of the SiC MOSFET and Si IGBT was not selected lower than 5 Ω to avoid a large voltage dip during the turn-on transition. It is found that the 5 Ω of R_{gon} and 15 Ω of R_{goff} will ensure an acceptable tradeoff between the switching energy losses, dv/dts and di/dts values, and the ringing in the voltage and current waveforms.

The switching energy losses are also characterized and measured for all of the power devices at different current levels. Fig. 19 demonstrates the turn-on, turn-off, and total switching energy losses for a range of switched current from 4 A to 20 A. The measurements are obtained at room temperature with 800 V of dc bus voltage. The R_{gon} and R_{goff} for all of the power devices are 5 Ω and 15 Ω, respectively. The SiC MOSFET and Si IGBT have substantial increases in energy losses at both the turn-on and turn-off transitions with current increases. Whereas, the SiC cascode features a lower pace of energy losses increasing with the current elevation. As the current changes from 4 A to 20 A, the turn-on energy loss is raised by a factor of more than 10, 8, and 4 of the Si IGBT, SiC MOSFET, and SiC cascode, respectively. While the turn-off transition experienced energy loss at 20 A by more than 5, 11, and 4 times than that at 4 A of the Si IGBT, SiC MOSFET, and SiC cascode, respectively. At switch currents of 12 A and below, the Si IGBT has a lower turn-on energy loss than the SiC MOSFET. Again, the SiC cascode features the smallest total switching energy loss among all the power devices within all the considered range of current due to its lower turn-on and turn-off energy losses. It is found that the total switching energy loss of the SiC cascode is nearly lower 4 times than that of the SiC MOSFET and almost 5 times lower than that of the Si IGBT at a current of 16 A. This is a very attractive aspect of the SiC cascode to counterbalance the losses that arise from high switching frequency operations.

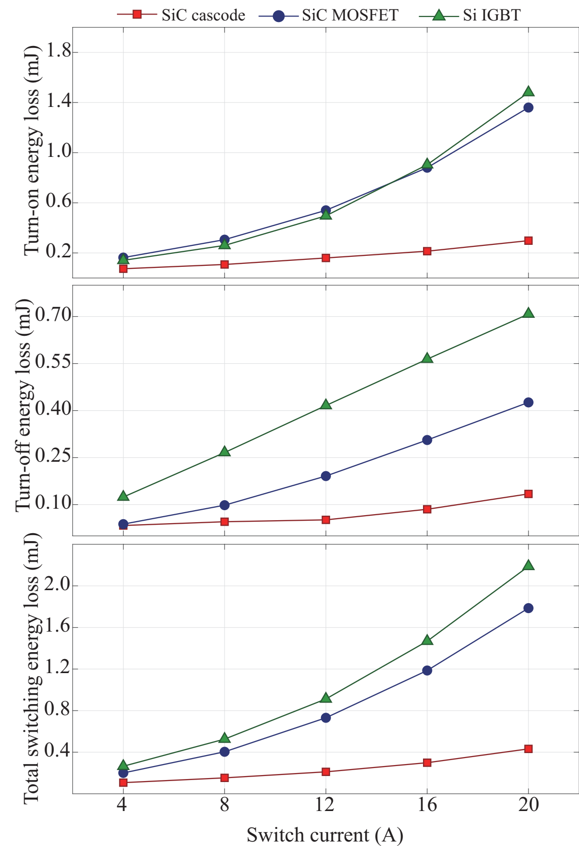

Fig. 19. Switching energy losses versus different switch current levels at: V_{dc} = 800 V, V_{gs} = +20/−5 V for the SiC cascode, V_{gs} = +15/−3 V for the SiC MOSFET, V_{gs} = +15/−5 V for the Si IGBT, turn-on gate resistance = 5 Ω and turn-off gate resistance = 15 Ω for all of the devices. Turn-on energy loss (top), turn-off energy loss (middle), total switching energy loss (bottom).

The effect of voltage dependency on energy losses is also studied under different blocking voltages. Fig. 20 provides the measurements at room temperature of the turn-on, turn- off, and total switching energy losses as the blocking voltage changes from 400 V to 800 V and with 15 A of switch current. For all of the power devices, the R_{gon} is 5 Ω while the R_{goff} is 15 Ω. It can been seen that at 600 V and beyond, the Si IGBT competes with the SiC MOSFET in terms of the turn-on energy loss, while there is a relative superiority of the SiC MOSFET below 600 V. As the voltage increases from 400 V to 800 V, the turn-on energy loss is increased by more than 6 times that of the SiC cascode and over 2 times that of the SiC MOSFET and Si IGBT.

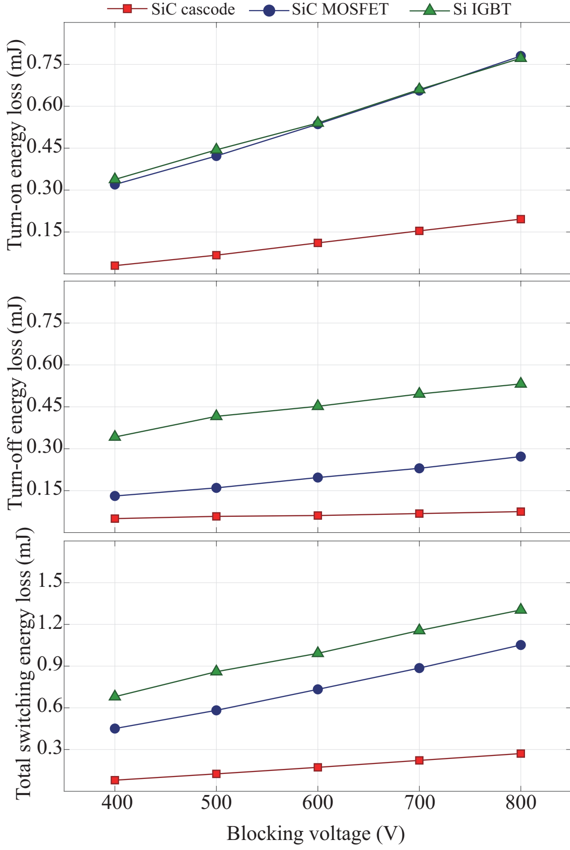

Fig. 20. Switching energy losses versus different blocking voltages at: I_d = 15 A, V_{gs} = +20/−5 V for the SiC cascode, V_{gs} = +15/−3 V for the SiC MOSFET, V_{gs} = +15/−5 V for the Si IGBT, turn-on gate resistance = 5 Ω and turn-off gate resistance = 15 Ω for all of the devices. Turn-on energy loss (top), turn-off energy loss (middle), total switching energy loss (bottom).

Meanwhile, the changes in the turn-off energy loss are recorded to be increasing by 1.5 times of the SiC cascode, over 2 times of the SiC MOSFET, and comparatively above 1.5 times of the Si IGBT. Even the SiC cascode exhibits the highest rate of turn-on energy loss increasing, both the SiC MOSFET and Si IGBT still need to dissipate almost 4 times the turn-on energy of the SiC cascode at 800 V. Furthermore, it can be seen that there is a weaker correlation among the turn-off energy loss and device blocking voltage. This is mainly attributed to the shorter turn-off time. Both the lower turn-on and turn-off energy losses of the SiC cascode drive it to feature the smallest total switching energy loss among all the power devices. From these provided loss profile data, the switching energy loss of power converters can be determined when operated under hard-switching conditions.

VI. Device Application and Assessment in a Hard-Switched Power Converter System

Based on the extracted device characteristics and behavior information, the power devices under study are experimentally assessed at converter level in this section. The major target is to quantify the potential of each device in the applications of hard-switched power converter systems. In this regard, a 800 W non-isolated dc-dc buck converter with 600–800 V of input voltage, v_{in}, and a 400 V of output voltage, v_{out}, is designed and built. For a fair comparison, the converter is operated in multiple iterations comparing each active power device in Table I. This ensures an identical operational environment in terms of the components as well as parasitic and stray inductances of the converter. Fig. 21 shows a simplified schematic diagram of the designed non-isolated dc-dc buck converter. In what follows, different design considerations are addressed.

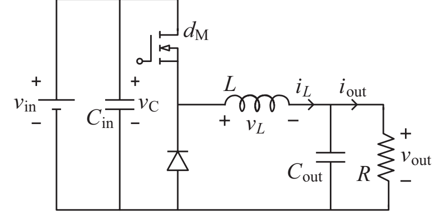

Fig. 21. Simplified schematic diagram of a non-isolated dc-dc buck converter.

The design process of a power converter requires close attention to many details so that the projected design outcomes can be met. The input-output specifications determine the appropriate converter topology for a particular application. Selection of power devices during the converter design is typically done through stress-level calculations. The reactive components are also crucial parts in the construction of any power converter. The inductor in Fig. 21, L, provides current stiffness in the output side of the converter. The overall power converter size is primarily constrained by the inductor. This is due to the fact that, in most power converters, the inductor represents usually the largest and heaviest element. Thus, a higher switching frequency helps to reduce both the inductor and overall converter sizes. Calculation of flux linkage variation in the L is performed through the integration of the instantaneous inductor voltage for a $d_M T_s$ of the switching period, T_s, where d_M is the duty cycle of the active switch. Then, the L is sized by

$$\Delta\lambda(v_{in}) = L(v_{in})\Delta i, \quad (1)$$

where $\Delta\lambda(v_{in})$ is the flux linkage variation in the L as a function of input voltage and Δi is the peak-to-peak current ripple in the inductor L, which is the design parameter. Similarly, in order to size the input and output capacitors, their electrical charges' variation are computed by the integration of the instantaneous current in these capacitors. Then, C_{in} and C_{out} are sized using

$$\Delta Q_{C_{in}}(v_{in}) = C_{in}(v_{in})\Delta v_{C_{in}}, \quad (2)$$

$$\Delta Q_{C_{out}}(v_{in}) = C_{out}(v_{in})\Delta v_{C_{out}}, \quad (3)$$

where $\Delta Q_{C_{in}}(v_{in})$ and $\Delta Q_{C_{out}}(v_{in})$ are the charges' variation as a function of input voltage in the C_{in} and C_{out}, respectively. $\Delta v_{C_{in}}$ and $\Delta v_{C_{out}}$ are the peak to peak ripple of the C_{in} and C_{out} voltages, which are the design parameters [24], [34]. The designed converter specifications and components are tabulated in Table IV.

The energy losses during the switching and conducting process increase the junction temperature (T_j) of a power device,

TABLE IV
COMPONENTS OF THE NON–ISOLATED DC-DC BUCK CONVERTER

Component	Manufacturer	Specifications
Input capacitor (C_{in})	Vishay, MKP1848C55012JK2	5 μF, ESR = 10 mΩ
Output capacitor (C_{out})	KEMET, C4ASPBU3470A3GJ	0.47 μF, ESR = 4.8 mΩ
Inductor (L)	Hammond Manufacturing, 195M10	20 mH × 3, ESR = 0.013 Ω
Load resistor (R)	TE Connectivity, TE1000B100RJ	100 Ω × 2

which may drive to a performance failure in the absence of an effective heat dissipation system. Therefore, design of a proper thermal management system is inevitable to ensure that the defined physical limits of the design components are not exceeded, thus enabling a maximum output power from the power converter. Calculation of power dissipation of a power device and selection of a proper heat sink can be done using

$$P_D = \frac{T_j - T_a}{R_{th,ja}}, \quad (4)$$

$$R_{th,ja} = R_{th,jc} + R_{th,cs} + R_{th,sa}, \quad (5)$$

where P_D, T_a, and $R_{th,ja}$ are the device power dissipation, the ambient temperature, and the total junction to ambient thermal resistance, respectively. It can be seen that from (5), $R_{th,ja}$ is a series combination of three independent thermal resistances, namely junction to case thermal resistance, $R_{th,jc}$, case to heat sink thermal resistance, $R_{th,cs}$, and heat sink to ambient thermal resistance, $R_{th,sa}$ [35]. The typical values of the $R_{th,jc}$ are 0.45 °C/W and 0.70 °C/W of the SiC cascode and SiC MOSFET, respectively. Also, the Si IGBT has a 0.70 °C/W of $R_{th,jc}$ as a maximum value. Here, a cooling system with forced air flow using a fan is arranged for cooling the heat sink as well as the inductor. Under this condition, a heat sink from Aavid Thermalloy, part number 057908, that has a 1.52 °C/W/3in of thermal resistance is used in the design. Further, it is worth mentioning that a ceramic thermal interface is used between each power device and the heat sink. This ceramic thermal interface is selected from Fischer Elektronik, part number AOS2182471, which is important to minimize the $R_{th,cs}$ value.

VII. EXPERIMENTAL VERIFICATION OF CONVERTER OPERATION AND EFFICIENCY

A laboratory experimental setup for evaluating the controlled power devices in Table V is depicted in Fig. 22. The parameters of the non-isolated dc-dc buck converter are listed in Table I. As mentioned earlier, for the sake of fair comparison, the converter is operated with each controlled power device, i.e., with SiC cascode, SiC MOSFET, and Si IGBT using the same reactive components. Also, a SiC Schottky diode from Cree, Inc., C4D15120D, is used with each aforementioned controlled

TABLE V
GATE DRIVING CONDITIONS

Power device	R_{gon} /Ω	R_{goff} /Ω	V_{gson}/V_{geon}/V	V_{gsoff}/V_{geoff}/V
SiC cascode	5	15	+20	–5
SiC MOSFET	5	15	+15	–3
Si IGBT	5	15	+15	–5

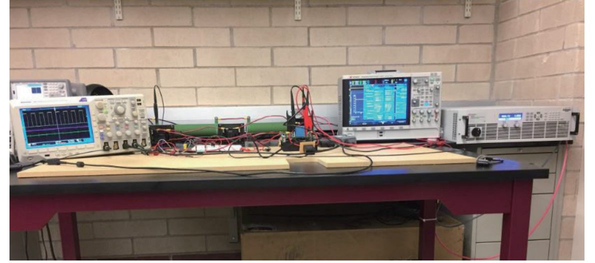

Fig. 22. Laboratory experimental setup of the 400 V output non-isolated dc-dc buck converter.

Fig. 23. Operation waveforms of the converter with the SiC cascode at 800 V of v_{in} and switching frequency of 20 kHz (top), 50 kHz (middle), and 100 kHz (bottom). Scale: V_{ds}, v_{out} → 250 V/div, i_{out} → 1 A/div, time → 40 μs/div.

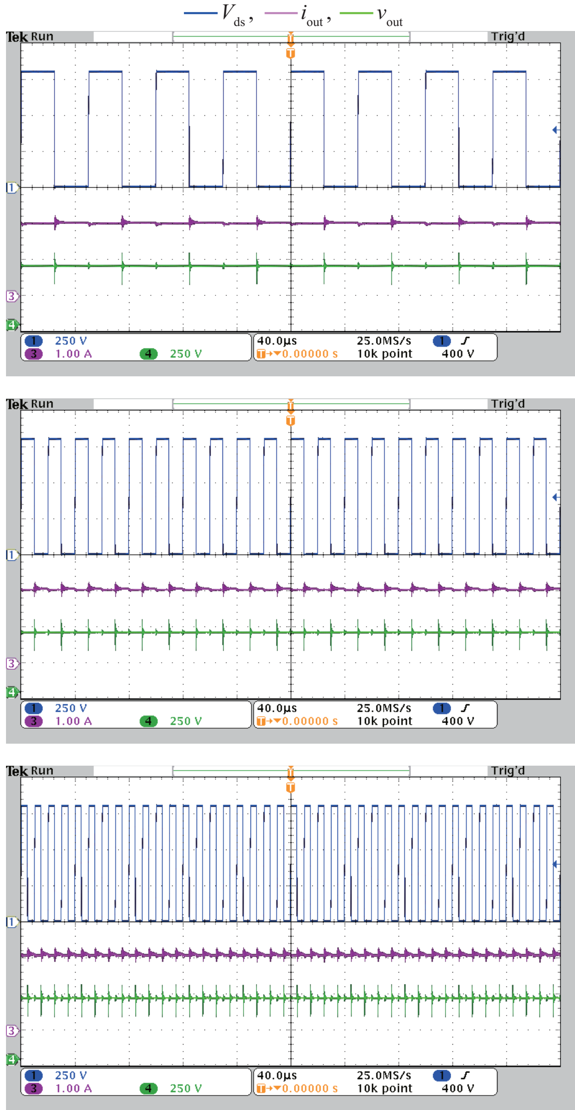

Fig. 24. Operation waveforms of the converter with the SiC MOSFET at 800 V of v_{in} and switching frequency of 20 kHz (top), 50 kHz (middle), and 100 kHz (bottom). Scale: V_{ds}, v_{out} → 250 V/div, i_{out} → 1 A/div, time → 40 μs/div.

Fig. 25. Operation waveforms of the converter with the Si IGBT at 800 V of v_{in} and switching frequency of 20 kHz (top), 50 kHz (middle), and 100 kHz (bottom). Scale: V_{ds}, v_{out} → 250 V/div, i_{out} → 1 A/div, time → 40 μs/div.

power device. A set of tests are conducted on the converter with each power device under open loop operation at a duty cycle of 0.5 and with a resistive load of 200 Ω. An isolated gate driver circuit consists of two isolated dc-dc converters, an ultrafast driver IC from IXYS, IXDN609SI, and an optocoupler is used to drive the power devices. Additionally, two diodes are used to realize separate driving paths for turn-on and turn-off conditions. The input signal to the gate driver circuit is provided by a single channel waveform generator 33500B from Keysight. The gate driving conditions of the power devices are summarized in Table V. The experimental operation waveforms of the converter with the SiC cascode, SiC MOSFET, and Si IGBT at 800 V of v_{in} and different switching frequencies are shown in Figs. 23, 24, and 25, respectively. Tektronix P5200A differential probes are used to measure the V_{ds} and v_{out}. The output current, i_{out}, is measured using an ELDITEST CP6770 current probe. It can be seen that each power device is successfully blocking the v_{in} value. Also, voltage and current ringing are observed in the v_{out} and i_{out} waveforms of the converter with each power device. These ringing are occurred at the turn-on instants of the power devices. It is to be noted that the converter with the SiC cascode exhibits the largest magnitude of ringing in the voltage and current.

The heat sink temperature of the converter with each power device is measured for the purpose of having a perception of the converter thermal condition. The heat sink temperatures of the converter with SiC cascode, SiC MOSFET, and Si IGBT are shown in Figs. 26, 27, and 28, respectively. These thermal images are captured after two minutes of converter operation with each power device under 800 V of v_{in} and at switching frequency values of 20, 50, and 100 kHz. The focus point in the heat sink, i.e., the indicator in the thermal images, is a close location to the power device. It is observed that the converter with the SiC cascode has the lowest rate of increase in heat

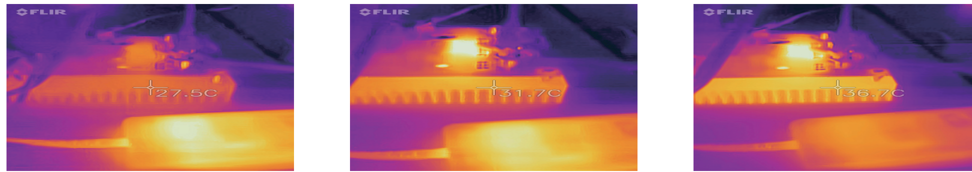

Fig. 26. Heat sink thermal image of the converter with the SiC cascode at 800 V of v_{in} and switching frequency of 20 kHz (left), 50 kHz (middle), and 100 kHz (right).

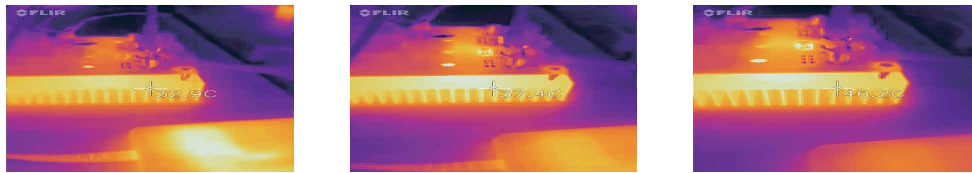

Fig. 27. Heat sink thermal image of the converter with the SiC MOSFET at 800 V of v_{in} and switching frequency of 20 kHz (left), 50 kHz (middle), and 100 kHz (right).

Fig. 28. Heat sink thermal image of the converter with the Si IGBT at 800 V of v_{in} and switching frequency of 20 kHz (left), 50 kHz (middle), and 100 kHz (right).

sink temperature as the switching frequency increases. When the switching frequency was increased from 20 kHz to 100 kHz, the heat sink temperature increased by roughly 33.454%, 40.425%, and 47.383% of the converter with the SiC cascode, SiC MOSFET, and Si IGBT, respectively. The lowest heat sink temperature of the SiC cascode based converter refers to the lowest power loss device.

The total power loss and efficiency measurements of the converter with each power device are experimentally collected through measuring the voltages and currents at the input and output sides of the converter. For this purpose, a Keysight IntegraVision power analyzer, model PA2203A, is employed. The voltage measurements with this equipment can be done without the need for differential probes. Also, the equipment enables direct current measurements employing built-in current shunts. Thus, it provides high-accuracy power measurements, with 0.05% basic accuracy and 0.1% best power accuracy, making it possible to capture small variations in the efficiency. Fig. 29 shows the total power loss and efficiency measurements of the converter with SiC cascode, SiC MOSFET, and Si IGBT at different values of v_{in} and switching frequency of 20 kHz. It can be seen that the converter with SiC cascode provides the lowest total power loss and highest efficiency compared to the SiC MOSFET and Si IGBT based converters. At 800 V of v_{in}, the efficiency of the SiC cascode based converter comes up to be 96.172%, while the efficiency of the converter with SiC MOSFET is 95.976% and it is 95.909% of the Si IGBT based converter. Fig. 30 depicts the measurements of the total power loss and efficiency of the converter with each power device at different values of switching frequency and 800 V of v_{in}. The SiC cascode based converter exhibits less total power loss

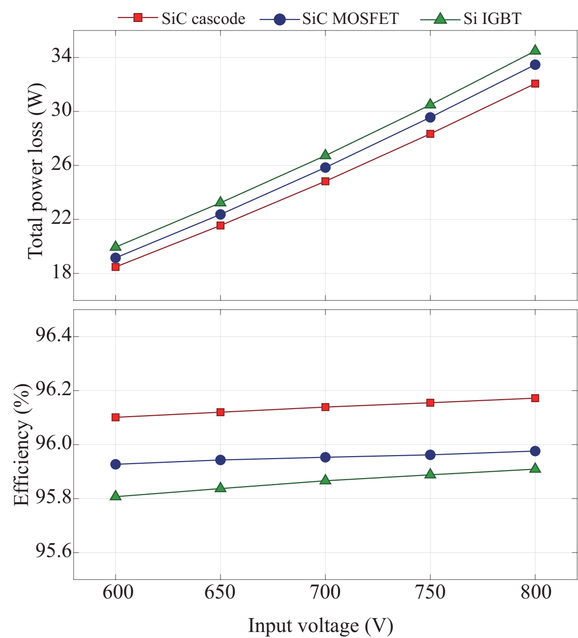

Fig. 29. Power loss and efficiency of the converter with the SiC cascode, SiC MOSFET, and Si IGBT at different values of v_{in} with 20 kHz of switching frequency.

within the tested switching frequency range, and therefore it is more efficient compared to the SiC MOSFET and Si IGBT based converters. Hence, when the SiC cascode is used in the construction of hard-switched dc-dc converters, it may bring major benefits in terms of efficiency improvements, decreasing reactive components' sizes, and reducing thermal design and cooling system requirements.

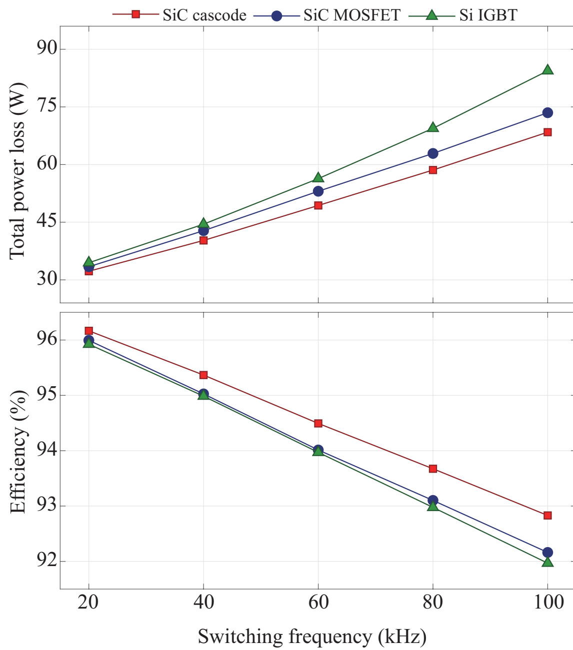

Fig. 30. Power loss and efficiency of the converter with the SiC cascode, SiC MOSFET, and Si IGBT at different switching frequencies with 800 V of v_{in}.

VIII. Conclusions

In this paper, an extensive experimental characterization study of the 1200 V SiC cascode, 1200 V SiC MOSFET, and 1200 V Si IGBT was presented. The key characteristics of the power devices were extracted under hard-switching conditions. Separated turn-on and turn-off gate driving paths were used to enable a thorough analysis of switching speeds and switching energy losses for the power devices. The switching performance of each power device under different R_{gon} and R_{goff} was reported and discussed. The voltage and current slopes of the SiC cascode are the steepest of the three, while its turn-off voltage overshoot is the largest. The switching energy analysis revealed that the SiC cascode exhibits lower turn-on and turn-off energy losses compared to the other two power devices. Such lower switching energy losses offer several advantages in terms of a more reliable converter design, a higher overall system efficiency, and a higher switching frequency operation under the same thermal design condition. Also, a strong dependence of the total switching energy loss on the R_{gon} was observed for all the power devices. Furthermore, it was shown that the switching speeds and gate resistance correlation during the turn-off transition of all three power devices is comparatively weaker than that during the turn-on transition. Based on switching performance analysis and switching energy losses considerations, best R_{gon} and R_{goff} values were identified. Moreover, to assess the potential of each power device in hard-switched converters, a non-isolated dc-dc buck converter was designed and experimentally studied. The operation, thermal condition, and efficiency of the converter with each power device were reported. The results demonstrated a superiority of the SiC cascode based converter against the SiC MOSFET and Si IGBT based converters. The presented results and provided analyses in this paper represent guidelines and prospects for loss expectation and advanced power converter systems design.

References

[1] Y. Bayar and H. A. Özel, "Electricity consumption and economic growth in emerging economies," in *Journal of Knowledge Management, Economics and Information Technology*, vol. 4, no. 2, pp. 1–18, 2014.

[2] IEA, "Global energy and CO_2 status report 2018," International Energy Agency, Tech. Rep., 2019.

[3] F. Appavou *et al.*, "Renewables 2019 global status report," Renewable Energy Policy Network for the 21*st* Century (REN21), Tech. Rep., 2019.

[4] V. Pathirana, N. Udugampola, T. Trajkovic, and F. Udrea, "Low-loss 800-V lateral IGBT in bulk Si technology using a floating electrode," in *IEEE Electron Device Letters*, vol. 39, no. 6, pp. 866–868, Jun. 2018.

[5] L. Zhang, J. Zhu, J. Ma, S. Cao, A. Li, Y. Zou, S. Li, W. Sun, J. Zhao, L. Shi, Y. Gu, and S. Zhang, "500-V silicon-on-insulator lateral IGBT with w-shaped n-typed buffer and composite p-typed collectors," in *IEEE Transactions on Electron Devices*, vol. 66, no. 3, pp. 1430–1434, Mar. 2019.

[6] S. H. Tran, L. Dupont, and Z. Khatir, "Electrothermal evaluation of single and multiple solder void effects on low-voltage Si MOSFET behavior in forward bias conditions," in *IEEE Transactions on Components, Packaging and Manufacturing Technology*, vol. 7, no. 3, pp. 396–404, Mar. 2017.

[7] S. Hazra, A. De, L. Cheng, J. Palmour, M. Schupbach, B. A. Hull, S. Allen, and S. Bhattacharya, "High switching performance of 1700-V, 50-A SiC power MOSFET over Si IGBT/BiMOSFET for advanced power conversion applications," in *IEEE Transactions on Power Electronics*, vol. 31, no. 7, pp. 4742–4754, Jul. 2016.

[8] J. Jordan, V. Esteve, E. Sanchis-Kilders, E. J. Dede, E. Maset, J. B. Ejea, and A. Ferreres, "A comparative performance study of a 1200 V Si and SiC MOSFET intrinsic diode on an induction heating inverter," in *IEEE Transactions on Power Electronics*, vol. 29, no. 5, pp. 2550–2562, May 2014.

[9] K. Shenai, "Future prospects of widebandgap (WBG) semiconductor power switching devices," in *IEEE Transactions on Electron Devices*, vol. 62, no. 2, pp. 248–257, Feb. 2015.

[10] J. W. Palmour, J. A. Edmond, H. S. Kong, and C. H. Carter, "6H–silicon carbide power devices for aerospace applications," in *Proceedings of* 28*th Intersociety Energy Conversions Engineering Conferrence (IECEC)*, vol. 1, Aug. 1993, pp. 1249–1254.

[11] S. Banerjee, T. P. Chow, and R. J. Gutmann, "1300-V 6H-SiC lateral MOSFETs with two RESURF zones," in *IEEE Electron Device Letters*, vol. 23, no. 10, pp. 624–626, Oct. 2002.

[12] S. Krishnaswami, A. Agarwal, Sei-Hyung Ryu, C. Capell, J. Richmond, J. Palmour, S. Balachandran, T. P. Chow, S. Bayne, B. Geil, K. Jones, and C. Scozzie, "1000-V, 30-A 4H-SiC BJTs with high current gain," in *IEEE Electron Device Letters*, vol. 26, no. 3, pp. 175–177, Mar. 2005.

[13] N. Miura, K. Fujihira, Y. Nakao, T. Watanabe, Y. Tarui, S. Kinouchi, M. Imaizumi, and T. Oomori, "Successful development of 1.2 kV 4H-SiC MOSFETs with the very low on-resistance of 5 mΩ cm2 ," in *Proceedings of 2006 IEEE International Symposium on Power Semiconductor Devices and IC's*, Jun. 2006, pp. 1–4.

[14] R. A. Wood and T. E. Salem, "Evaluation of a 1200-V, 800-A all-SiC dual module," in *IEEE Transactions on Power Electronics*, vol. 26, no. 9, pp. 2504– 2511, Sept. 2011.

[15] C. Chen, Y. Chen, Y. Li, Z. Huang, T. Liu, and Y. Kang, "An SiC-based half-bridge module with an improved hybrid packaging method for high power density applications," in *IEEE Transactions on Power Electronics*, vol. 64, no. 11, pp. 8980–8991, Nov. 2017.

[16] R. Singh, J. A. Cooper, M. R. Melloch, T. P. Chow, and J. W. Palmour, "SiC power schottky and PiN diodes," in *IEEE Transactions on Electron Devices,* vol. 49, no. 4, pp. 665–672, Apr. 2002.

[17] A. Elasser, M. H. Kheraluwala, M. Ghezzo, R. L. Steigerwald, N. A. Evers, J. Kretchmer, and T. P. Chow, "A comparative evaluation of new silicon carbide diodes and state-of-the-art silicon diodes for power electronic applications," in *IEEE Transactions on Industry Applications*, vol. 39, no. 4, pp. 915– 921, Jul. 2003.

[18] G. Spiazzi, S. Buso, M. Citron, M. Corradin, and R. Pierobon, "Performance evaluation of a Schottky SiC power diode in a boost PFC application," in *IEEE Transactions on Power Electronics*, vol. 18, no. 6, pp. 1249–1253, Nov. 2003.

[19] M. Schweizer, T. Friedli, and J. W. Kolar, "Comparison and implementation of a 3-level NPC voltage link back-to-back converter with SiC and Si diodes," in *Proceedings of 2010 Twenty-Fifth Annual IEEE Applied Power Electronics Conference and Exposition (APEC)*, Feb. 2010, pp. 1527–1533.

[20] R. Wu, J. O. Gonzalez, Z. Davletzhanova, P. A. Mawby, and O. Alatise, "The potential of SiC cascode JFETs in electric vehicle traction inverters," in *IEEE Transactions on Transportation Electrification*, vol. 5, no. 4, pp. 1349–1359, 2019.

[21] K. Zhu, M. O'Grady, J. Dodge, J. Bendel, and J. Hostetler, "1.5 kW single phase CCM totem-pole PFC using 650V SiC cascodes," in *Proceedings of 2016 IEEE 4th Workshop Wide Bandgap Power Devices and Applications (WiPDA)*, 2016, pp. 90–94.

[22] K. Koiwa and J. Itoh, "A maximum power density design method for nine switches matrix converter using SiC-MOSFET," in *IEEE Transactions on Power Electronics*, vol. 31, no. 2, pp. 1189–1202, Feb. 2016.

[23] D. Dong, M. Agamy, G. Mandrusiak, and Q. Chen, "Design of high-speed H-bridge converter using discrete SiC MOSFETs for solid-state transformer applications," in *Proceedings of 2017 IEEE Energy Conversion Congress and Exposition (ECCE)*, Oct. 2017, pp. 1379–1386.

[24] A. M. S. Al-bayati, S. S. Alharbi, S. S. Alharbi, and M. Matin, "A comparative design and performance study of a non-isolated DC-DC buck converter based on Si-MOSFET/Si-diode, SiC-JFET/SiC-schottky diode, and GaN-transistor/SiC-schottky diode power devices," in *Proceedings of 2017 North American Power Symposium (NAPS)*, Sept. 2017, pp. 1–6.

[25] O. Kwon, J. Kwon, and B. Kwon, "Highly efficient single-phase three-level three-leg converter using SiC MOSFETs for AC-AC applications," in *IEEE Transactions on Power Electronics*, vol. 65, no. 9, pp. 7015–7024, Sept. 2018.

[26] K. Vechalapu, S. Bhattacharya, E. V. Brunt, S. H. Ryu, D. Grider, and J. W. Palmour, "Comparative evaluation of 15-kV SiC MOSFET and 15-kV SiC IGBT for medium-voltage converter under the same d*v*/d*t* conditions," in *IEEE Journal of Emerging and Selected Topics in Power Electronics*, vol. 5, no. 1, pp. 469–489, Mar. 2017.

[27] H. Akagi, S. Kinouchi, and Y. Miyazaki, "Bidirectional isolated dual-active-bridge (DAB) DC-DC converters using 1.2-kV 400-A SiC-MOSFET dual modules," in *CPSS Transactions on Power Electronics and Applications*, vol. 1, no. 1, pp. 33–40, Dec. 2016.

[28] Z. Chen, D. Boroyevich, R. Burgos, and F. Wang, "Characterization and modeling of 1.2 kV, 20 A SiC MOSFETs," in *Proceedings of 2009 IEEE Energy Conversion Congress and Exposition*, Sept. 2009, pp. 1480–1487.

[29] R. Pittini, Z. Zhang, and M. A. Andersen, "SiC JFET cascode loss dependency on the MOSFET output capacitance and performance comparison with trench IGBTs," in *Proceedings of 2013 Twenty-Eighth Annual IEEE Applied Power Electronics Conference and Exposition (APEC)*, 2013, pp. 1287–1293.

[30] C. M. DiMarino, R. Burgos, and B. Dushan, "High-temperature silicon carbide: characterization of state-of-the-art silicon carbide power transistors," in *IEEE Industrial Electronics Magazine*, vol. 9, no. 3, pp. 19–30, Sept. 2015.

[31] K. Peng, S. Eskandari, and E. Santi, "Characterization and modeling of a gallium nitride power HEMT," in *IEEE Transactions on Industry Applications*, vol. 52, no. 6, pp. 4965–4975, Nov. 2016.

[32] J. Lutz, H. Schlangenotto, U. Scheuermann, and R. De Doncker, *Semiconductor power devices – physics, characteristics, reliability*. New York, NY, USA: Springer-Verlag, 2011, p. 320.

[33] N. Oswald, P. Anthony, N. McNeill, and B. H. Stark, "An experimental investigation of the tradeoff between switching losses and EMI generation with hard-switched all-Si, Si-SiC, and all-SiC device combinations," in *IEEE Transactions on Power Electronics*, vol. 29, no. 5, pp. 2393–2407, May 2014.

[34] N. Mohan, *Power electronics A first course*. John Wiley & Sons, Inc., 2012, pp. 38–73.

[35] S. Lee, "Optimum design and selection of heat sinks," in *IEEE Transactions on Components, Packaging, and Manufacturing Technology: Part A*, vol. 18, no. 4, pp. 812–817, Dec. 1995.

Ali Mahmoud Salman AL-Bayati received the B.Sc. and M.Sc. degrees in electrical engineering from the University of Baghdad, Baghdad, Iraq, in 2007 and 2010, respectively. He completed Ph.D. degree in electrical and computer engineering in Daniel Felix Ritchie School of Engineering and Computer Science, University of Denver, Denver, Colorado, USA, in 2021. His research interests include wide bandgap semiconductors' characterization and application, power electronic converter systems, renewable energy integration.

Mohammad Abdul Matin is the Professor of electrical and computer engineering, in the School of Engineering and Computer Science, University of Denver. He did B.S. (Honors) and M.S. in applied physics and electronics with First Class from Dhaka University, Bangladesh and Ph.D. in electrical and electronics engineering from Nottingham University in England in 1993. He then joined as Post-Doctoral Fellow (94−95), Research Engineer (95−98) at the Center for Electro photonics Materials and Devices, McMaster University, Hamilton Canada. He moved to the University of Toronto, Canada as Senior Research Associate (1998−2000). In March 2000 he joined as an Assistant Professor of Electrical Engineering, in the School of Engineering and Computer Science, He is a Senior Member of IEEE, OSA & SPIE and member of ASEE and Sigma Xi. His research interests are in power electronics and optoelectronic materials, devices and systems, optical & bio–medical signal & image processing.